Lawrence Berkeley National Laboratory
Recent Work

Title

PHOTOEMESSION FROM Cu VALENCE BANDS USING 50 - 175 eV SYNCHROTRON RADIATION

Permalink

https://escholarship.org/uc/item/9pr2c3bt

Author

Stohr, J.

Publication Date

1976-02-01

000045035467

PHOTOEMISSION FROM Cu VALENCE BANDS
USING 50 - 175 eV SYNCHROTRON RADIATION

J. Stöhr, F. R. McFeely, G. Apai,
P. S. Wehner, and D. A. Shirley

February 1976

LBL-4925
c.1

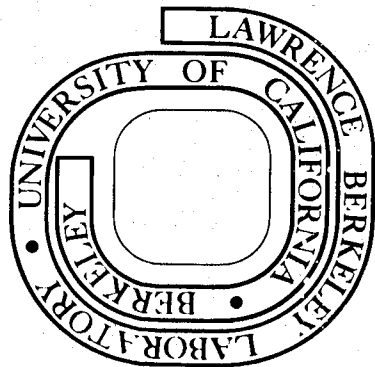# DISCLAIMER

Photoemission from Cu Valence Bands Using 50 - 175 eV Synchrotron Radiation*

J. Stöhr, F. R. McFeely, G. Apai, P. S. Wehner, and D. A. Shirley

Materials and Molecular Research Division
Lawrence Berkeley Laboratory

and

Department of Chemistry

University of California
Berkeley, California 94720

February 1976

ABSTRACT

Photoemission spectra of the 3d valence band of polycrystalline Cu were studied using synchrotron radiation of energy 50 eV $\leqslant$ hν $\leqslant$ 175 eV. The detailed shape of the spectrum was found to change distinctly with photon energy. The observed energy dependence was compared to calculated photoemission energy distributions (PED's) assuming a direct transition model. PED's obtained with this model predicted the experimental intensity distribution quite well for hν < 70 eV and hν > 120 eV but failed in the region h$\nu \approx$ 90 eV. Fair agreement between experiment and theory was obtained when momentum broadening in the final state was included. The largest broadening was required around hν = 90 eV. A minimum in the photoelectron mean free path at this energy is discussed as a possible source of broadening. The observed changes in spectral shape for 50 eV $\leqslant$ hν $\leqslant$ 70 eV are attributed to direct transitions; the changes are found to arise mainly from the angular part of the transition matrix element.

I. INTRODUCTION

The photoemission energy distribution (PED) which is obtained by

exciting valence electrons in solids depends mainly on three quantities:

the initial density of states, the photoexcitation matrix element, and

the final density of states. The latter two define the photoemission

cross-section. In the past two basic types of cross section effects

have been reported in photoemission spectroscopy of solids. In x-ray

photoemission spectroscopy (XPS) frequency dependent variations in photo-

emission intensity from s-, p-, d-, and f- derived valence electrons have

been observed.[1] They arise from different radial matrix elements for the

respective transitions.[1] In ultraviolet photoemission spectroscopy (UPS)

variations with photon energy in the PED's obtained by exciting valence

electrons are usually discussed in terms of final state effects which

are responsible for the observed line positions and transition matrix

element modulations that determine the line intensities.[1]

The photoemission studies on Cu (3d) valence electrons reported

here are in a sense a simple extension of the UPS studies mentioned

above. However, at the photon energies (50 eV - 175 eV) used for our

angle integrated experiments on polycrystalline samples, several new

phenomena arise. In raising the photon energy the number of accessible

final states increases.[2] While in the UPS regime transitions occur only

at special $\vec{k}$ points of the Brillouin zone (BZ) at higher photon energies

a considerably larger part of the zone is sampled. Therefore the positions

of the peaks which constitute the PED predominantly reflect the initial

density-of-states structure and are expected to remain essentially un-

shifted. The peak intensities on the other hand may change significantly

with photon energy because of both the angular and radial parts of the transition matrix element. The study of these intensity changes with frequency is the main purpose of the present paper.

In contrast to the situation that prevails in the UPS regime, one other point is of considerable interest at higher photon energies. The photoelectron mean free path of most materials exhibits a broad minimum around 100 eV.[3] As discussed by Feibelman and Eastman[4] such inelastic damping which restricts the source region of the photocurrent near the surface results in an uncertainty or spread of the final state momentum component perpendicular to the surface.

In the following Sections IIa and IIb we describe the experimental arrangement and results, respectively. In Section IIIa we present a simple model to calculate the Cu 3d PED's under the assumption of direct optical transitions. In Section IIIb we show how to include momentum broadening in the final state in a simple stochastic fashion. We discuss the results of such calculations in Sections IVa and IVb. In the concluding Section V we consider some future problems which have been stimulated by the present investigation.

II. EXPERIMENT

A. Experimental Arrangement

Experiments were performed using synchrotron radiation from the storage ring SPEAR at the Stanford Linear Accelerator (SLAC). The ultra-high vacuum grazing incidence monochromator has been described in detail elsewhere.[5] Photoelectrons were detected by a double pass, electrostatic deflection cylindrical mirror analyzer (CMA) operated in the retarding mode (constant resolution 0.35 eV).[6] Samples were prepared by in situ

evaporation of Cu from a tungsten filament onto a stainless steel sub-
strate. The maximum pressure reached during evaporation was 2×10^{-8}
Torr. Experiments were carried out at $\sim 1 \times 10^{-9}$ Torr.

B. Experimental Results

Experimental results for Cu are displayed in Figure 1. Common
features of all spectra are the three peaks at ~ 2.4 eV, ~ 3.5 eV, and
~ 4.6 eV binding energy (BE) relative to the Fermi level. The most dis-
tinct changes in the shape of the VB spectra occur between 50 and 70 eV.
While the peak positions remain essentially unshifted the intensity of
the peak at 3.5 eV BE increases with photon energy. Above 70 eV this
trend continues in a less spectacular way. At the highest photon energies
the spectra seem to approach the PED observed with $A\ell$ K_α radiation[7]
(compare Figure 2a).

III. THEORY

A. The Direct Transition Model

For the calculation of the PED's we have employed the familiar three
step model of photoemission.[8] We assume independent excitation, trans-
port and escape processes. The excitation process from an initial state
j to a final state f at a general point $\vec{k}$ of the Brillouin zone is
described by a matrix element $t_{fj}(\vec{k})$. The matrix element is calculated
in the dipole velocity approximation under the assumption of crystal
momentum conservation during the excitation process (cp. Appendix A).
Transport of the excited photoelectron to the surface is described by
a term $D_f(\vec{k})$ which is proportional to the group velocity of the electron
(cp. Appendix B). In our case of angle-integrated photoemission with
final state energies much larger than the initial state band width a

surface transmission term may be neglected. The PED is then given by[1]

$$N(E, \hbar\omega) \sim \int_{BZ} d^3k \sum_{j,f} D_f(\vec{k}) \, |t_{fj}(\vec{k})|^2 \, \delta(E_f(\vec{k}) - E_j(\vec{k}) - \hbar\omega) \, \delta(E - E_j(\vec{k})) \tag{1}$$

Details of the k- integration are discussed in Appendix C. The term $|t_{fj}(\vec{k})|^2 \, \delta(E_f(\vec{k}) - E_j(\vec{k}) - \hbar\omega)$ in equation (1) corresponds to the photo-emission cross section. Let us discuss it first.

Evaluation of the cross section term requires the knowledge of init-ial- and final-state energies and wave functions. At excitation energies larger than 50 eV the description of the final Bloch state is a non-trivial problem, as band structure calculations generally do not exist at such high energies.[9] We shall therefore describe our final state by a free-electron model, for which the eigenvalues in the reduced zone scheme are given by[10]

$$E_f(\vec{k}) = \frac{\hbar^2}{2m} \, |\vec{k} + \vec{G}|^2 \tag{2}$$

Here $\vec{k}$ is the crystal momentum within the first BZ and $\vec{G}$ is a reciprocal lattice vector. The "zero" of our free electron energy bands was adjust-ed to the bottom of the 4s type bands obtained from a tight-binding cal-culation described below. The final state wave function is taken to be an orthogonalized plane wave (OPW), also discussed in more detail below and in Appendix A. Smith's[11] parameterization of the linear combination of atomic orbital (LCAO) interpolation scheme of Hodges, Ehrenreich, and Lang[12] was adopted to yield the initial-state energies $E_j(\vec{k})$ and the coefficients $a_m^j(\vec{k})$ for the corresponding wave functions[12]

$$|j> = N^{-1/2} \sum_{\ell,m} e^{i\vec{k}\cdot\vec{R}_\ell} \, a_m^j(\vec{k}) \, D_m(\vec{r} - \vec{R}_\ell) \tag{3}$$

Here $D_m(\vec{r}) = R_d(r) \, d_m(\Theta_r, \phi_r)$ are atomic d-wave functions. The real angular functions $d_m(\Theta, \phi)$ are tabulated in Table I of Reference 13. The radial parts $R_d(r)$ in the form of Slater orbitals were taken from Reference 14. Equation (3) is the d-projection of the total LCAO wave function. For our calculation the s-part of the initial state wave function has been neglected because its transition matrix element is relatively small. The sum in equation (3) extends over the five angular d-functions and neighbor positions $\vec{R}_\ell$ in the fcc lattice. Assuming an OPW final state the matrix element $t_{fj}(\vec{k}) = \langle f|\vec{A}\cdot\vec{p}|j \rangle$ may be evaluated as (Appendix A)

$$|t_{fj}(\vec{k})|^2 \sim c^2 \sum_{\vec{G}} \left| \sum_m a_m^j(\vec{k}) \, \vec{A}\cdot\left[\vec{q} \, D_m(\vec{q}) + \sum_n P_n(\vec{q}) \, \vec{M}_{mn}\right] \right|^2 \delta(\vec{k} + \vec{G} - \vec{q})$$

(4)

Here C is a normalization constant for the OPW (equation A2), $\vec{G}$ is a reciprocal lattice vector, $\vec{A}$ is the vector potential and $\vec{q} = \vec{k} + \vec{G}$ is the wave vector of the photoelectron. The sum over n involves all wave functions of occupied atomic states $P_n(\vec{r})$ for which the transition matrix element $\vec{M}_{mn} = \langle D_m(\vec{r})|\vec{\nabla}|P_n(\vec{r}) \rangle$ (compare Appendix A) does not vanish. In our case of photoemission from 3d states only the atomic 2p and 3p functions need to be considered. $D_m(\vec{q}) = f_d(q) \, d_m(\Theta_q, \phi_q)$ and $P_n(\vec{q}) = f_p(q) \, p_n(\Theta_q, \phi_q)$ are Fourier transforms of the atomic d and p wave functions $D_m(\vec{r})$ and $P_n(\vec{r})$ respectively (Appendix A). The functions $p_n(\Theta, \phi)$ are listed in Table III of Reference 13. The δ-function in equation (4) represents the direct transition requirement of momentum conservation. For polycrystalline samples effects of light

polarization may be neglected in evaluating equation (4).

B. Momentum Broadening in the Final State

The direct transition model presented above may easily be extended to include momentum broadening in the final state. While the physical reasons for such an extension are discussed in more detail below we will at this point present a simple stochastic way to include momentum broadening in the calculation. The idea of momentum broadening is to smear only the _direction_ of the final state momentum vector $\vec{q}$ (i.e. the angles ϕ_q and Θ_q). The _absolute_ _value_ $|\vec{q}|$, which also defines the final state energy, is conserved. We employ the same equations as for the direct-transition case, except that we are less restrictive in the description of the final state. For a given free electron final state $\vec{k} + \vec{G}$ we allow all final states with wave vectors $\vec{p}$ and energy $E'_f(\vec{k}) = \frac{\hbar^2}{2m} |\vec{p}|^2$ which satisfy $(\vec{k} + \vec{G}) - \vec{\Delta}/2 \leqslant \vec{p} \leqslant (\vec{k} + \vec{G}) + \vec{\Delta}/2$ and the energy conserving δ-function $\delta(E'_f(\vec{k}) - E_j(\vec{k}) - \hbar\omega)$ in equation (1). Since our calculations apply for a polycrystalline sample we assume all directions $(\vec{k} + \vec{G})_i$ ($i = x,y,z$) to be equally broadened where $\Delta_i = |\vec{k} + \vec{G}| B/100$. The broadening parameter B is chosen to minimize the difference between experimental and calculated PED's. The effect of the broadening factor B is to create more possible final states at a given $\vec{k}$ point. While all _allowed_ final states are required to have the same energy $E'_f(\vec{k})$ they are, however, characterized by different momentum vectors $\vec{p}$. Except for substituting $E'_f(\vec{k})$ for $E_f(\vec{k})$ in equation (1) and $\vec{p}$ for $\vec{k} + \vec{G}$ in equation (4) the momentum-broadening and direct-transition calculations are identical.

IV. RESULTS AND DISCUSSION

A. Direct Transitions

Results of the calculation assuming direct transitions (compare Appendix C) are shown in Figure 3a. The calculation predicts essentially constant peak positions; i.e., the three-peak structure mentioned earlier, over the entire energy range, in complete agreement with experiment. When compared to the experimental PED's in Figure 3b (which have been corrected for inelastic background) reasonable agreement in peak intensities exists for $h\nu < 70$ eV and $h\nu \geqslant 120$ eV. The observed peak intensities are not reproduced well around $h\nu = 90$ eV.

It is interesting to explore the origin of the calculated changes in peak intensities. At a general $\vec{k}$ point the final state of an allowed direct transition (i.e. $E_f(\vec{k}) = E_j(\vec{k}) + \hbar\omega$) is characterized by a reciprocal lattice vector $\vec{G}$ (compare equation (2)).[10] Because of the δ-function in equation (4) the direction of $\vec{G}$ also fixes the direction of $\vec{q} = \vec{k} + \vec{G}$, i.e., the direction along which the photoelectron is allowed to leave.[16] The direction of $\vec{q}$ enters through the angular terms of the Fourier integrals $D_m(\vec{q})$ and $P_n(\vec{q})$ in equation (4) and it is this angular dependence which largely determines $|t_{fj}(\vec{k})|^2$. This is especially true for Cu since the 3d wave function does not have a radial node.[17] Figure 4 shows a plot of the angle averaged radial dipole matrix element squared (compare equation A17) versus the kinetic energy of the photoelectron. It is seen that the energy dependence of the radial part of equation (4) is negligible over the width (~ 3 eV) of the 3d valence band. Thus, only the angular part of the transition matrix element can cause changes in relative peak intensities within the Cu valence band. The

differences in peak intensities with photon energy is then easily under-
stood in our model. At different photon energies the final states at a
given $\vec{k}$ point will be characterized by different $\vec{G}$ vectors, leading to
different angular matrix elements.

The effect of the angular as compared to the radial matrix element
is demonstrated in Figure 5. Here a calculation with an <u>angle integrated</u>,
or because of the reasons given above essentially <u>constant</u> matrix elements
$\overline{|t_{fj}|}^2$ (dashed curve), is compared with a calculation including the
total matrix element $|t_{fj}|^2$ (solid curve) for $h\nu = 50$ eV and $h\nu = 90$ eV.
The former calculation yields similar results at both photon energies
while the latter shows strong modulation effects. The difference in
the angle integrated curves at $h\nu = 50$ eV and $h\nu = 90$ eV is a consequence
only of final-state effects, which arise through the energy conserving
function $\delta(E_f(\vec{k}) - E_j(\vec{k}) - \hbar\omega)$ in equation (1).

It is interesting to note the spectral variations implied by our
model at higher photon energies. As the photon energy is raised the
number of available final states increases. In the limit of large photon
energy this causes the PED's to resemble the initial-state band structure
shown in Figure 2b. In the high-photon-energy limit, modulation effects
due to the transition matrix element are also expected to be small,
because the various allowed final states result in an effective angular
integration. At this point we note that Nemoshkalenko et al.[18] included
angle-integrated matrix elements to account for the discrepancy between
the measured Cu XPS valence band spectrum and the calculated density of
states. They claimed that this discrepancy arises because electrons
with e_g symmetry have a higher transition probability than those with

t_{2g} symmetry. Our expression for the angle-integrated matrix element
(compare equation (A17)) is in disagreement with their result. Further-
more, equation (A17) reveals that for a <u>polycrystalline sample</u> the e_g
and t_{2g} components of the density of states cannot be distinguished
from one another. However, such a separation is possible in <u>angle-
resolved</u> photoemission from <u>single crystals,</u> which has been reported
for the cases of Ag and Au using Aℓ K_α radiation.[19]

B. Momentum Broadening in the Final State

In Figure 3c we present the results of a calculation in which
momentum broadening in the final state has been included. We have
chosen the respective broadening factors listed in Figure 3c to achieve
optimum agreement between the calculated and experimental (Figure 3b)
PED's. Except for $h\nu$ = 120 eV all calculated curves were found to be
quite sensitive to the choice of B, a finding which is demonstrated
in more detail in Figure 6. The calculated PED's including $\vec{k}$-broaden-
ing in the final state (Figure 3c) are found to be in good agreement
with the experimental spectra shown in Figure 3b, except for the slightly
too-pronounced peak structure. However, this difference arises entirely
from the initial state bandstructure rather than from cross section
effects. This is confirmed by Figure 2b where the Cu 3d density of
states (compare Appendix C, equation (C1)) is compared to the density of
states measured with Aℓ K_α radiation (Figure 2a). Note that the peak
structure is too pronounced generally and in particular the middle peak
is too high.

The success of our calculation, which includes momentum broadening
in the final state in describing the experimental PED's is striking.

Its description of the experimental spectra is considerably better than that obtained by the pure direct transition model. The fundamental difference between the two theoretical models lies in the description of the final state. To some extent the momentum broadening calculation covers up inadequacies in the description of the final state. It may be argued that the direct transition model does not reproduce the experimental spectra very well because of a poor description of the final state. This is indeed a problem since mixing of the various free-electron final states by the crystal potential has been ignored. The inclusion of momentum broadening somewhat simulates these effects. A direct-transition calculation of the kind presented here is not a stringent test because we are dealing with angle-integrated photoemission from a polycrystalline sample. In this case the whole BZ is sampled because all allowed transitions are also detected.

Despite the simplicity of the final state description employed in our direct transition calculation it is nevertheless very interesting to explore a possible physical reason for momentum broadening in the final state. As has been discussed in detail by Feibelman and Eastman[4] and recently by Grobman, Eastman, and Freeouf[20] and Feuerbacher and Willis,[21] momentum broadening in the final state may arise from a minimum in the photoelectron mean free path. Such a minimum is indeed known to occur in the energy range studied in the present investigation.[3] The magnitude of the broadening factors in Figure 3c indicate that the region of highest surface sensitivity occurs around hν = 90 eV (or a final state kinetic energy of ∿87 eV), which agrees remarkably well with the minimum of the mean-free-path <u>versus</u> energy curve in Reference 3. It is interest-

ing that in the energy range which is most highly surface sensitive the PED's resemble the one-electron density of states of the bulk. Final-state momentum broadening thus tends to weaken angular matrix element effects in photoemission. This is also clearly revealed by the model calculation in Figure 6.

V.   CONCLUSION

The experiments and calculations presented here may be regarded as a step toward understanding the influence of cross section and surface effects which arise in the transition region between UPS and XPS. An extension of such studies to other systems, in particular to 4d and 5d metals,[22] seems to be very promising. Angle-resolved photoemission from single crystals in the soft x-ray range is another interesting problem which might help to clarify the role of cross-section and/versus surface effects. Finally, we hope that calculations which treat photoemission as a scattering problem[23] may be stimulated by the present investigation. Experimental and theoretical investigations of this kind seem to be most important in contributing to a quantitative understanding of the photoemission process per se in solids.

APPENDIX A: DIPOLE MATRIX ELEMENTS

In evaluating the dipole matrix element $t_{fj}(\vec{k}) = <f|\vec{A}\cdot\vec{p}|j>$ we follow Gadzuk[13] except that we assume an OPW instead of a plane wave (PW) final state. The initial state $|j>$ is given by equation (3). The OPW final state is

$$|f> = C \left\{ |PW> - \sum_n < P_n(\vec{r})| PW > |P_n(\vec{r}) > \right\} \qquad (A1)$$

where

$$C = (< PW | PW > - \sum_n | < P_n(\vec{r})| PW > |^2)^{-1/2} \qquad (A2)$$

As has been discussed in Section IIIa the sum over n involves the atomic p-functions only. Following Gadzuk[13] the matrix element $t_{fj}(\vec{k})$ may now be readily evaluated in the dipole velocity approximation ($\vec{p} = -i\hbar\vec{\nabla}$) to yield equation (4).

The evaluation of the Fourier transforms $D_m(\vec{q})$ and $P_n(\vec{q})$ and the matrix element $\vec{M}_{mn}$ which occur in equation (4) should be discussed in more detail. The atomic d function has the general form

$$D_m(\vec{r}) = R_d(r) \, d_m(\Theta_r, \phi_r) \qquad (A3)$$

For Cu(3d) the radial part has the general Slater form

$$R_d(r) = ar^2 e^{-\alpha r} \qquad (A4)$$

The atomic p functions are

$$P_m(\vec{r}) = R_p(r) \, p_m(\Theta_r, \phi_r) \qquad (A5)$$

The radial part of the 2p and 3p functions can be written

$$R_p(r) = cre^{-\gamma r} + dr^2 e^{-\delta r} \tag{A6}$$

For our calculations the coefficients for the radial parts of the p and d wave functions were taken from Reference 14. The Fourier transforms of the atomic d-function (A3) is

$$D_m(\vec{q}) = \int d^3r \ e^{-i\vec{q}\cdot\vec{r}} \ D_m(\vec{r}) \tag{A7}$$

$$= f_d(q) \ d_m(\Theta_q, \phi_q) \tag{A8}$$

where

$$f_d(q) = -4\pi \int r^2 \ j_2(qr) \ R_d(r)dr \tag{A9}$$

For the atomic p functions the Fourier transform is

$$P_m(\vec{q}) = \int d^3r \ e^{-i\vec{q}\cdot\vec{r}} \ P_m(\vec{r}) \tag{A10}$$

$$= f_p(q) \ p_m(\Theta_q, \phi_q) \tag{A11}$$

where

$$f_p(q) = -4\pi i \int r^2 \ j_1(qr) \ R_p(r)dr \tag{A12}$$

The functions $j_1(qr)$ in equations (A9) and (A12) are spherical Bessel functions.[24]

The matrix element

$$\vec{M}_{mn} = \ < D_m(\vec{r})| \ \vec{\nabla} \ | \ P_n(\vec{r}) > \tag{A14}$$

may be separated into a radial and angular part according to

$$\vec{M}_{mn} = \vec{L}_{mn} \, h_{dp} \qquad \text{(A15)}$$

All non-vanishing components of $\vec{L}_{mn}$ are listed in Table I. The radial integral h_{dp} is given by

$$h_{dp} = \; < R_d(r) \, | \, \frac{\partial}{\partial r} - \frac{1}{r} \, | \, R_p(r) > \qquad \text{(A16)}$$

and its evaluation is straight forward.

Finally, the result for the angle integrated quantity $\overline{|t_{fj}(\vec{k})|^2}$ should be given. A lengthy but relatively easy calculation neglecting effects of light polarization[15] yields

$$\overline{|t_{fj}(\vec{k})|^2} \sim c^2 \Big\{ 5(f_d(q))^2 \, q^2$$
$$+ \, 2(f_p(q))^2 \, h_{dp}^{\;2}$$
$$+ \, 4f_d(q) \, f_p(q) \, q \, h_{dp} \Big\} \sum_m |a_m^j(\vec{k})|^2 \qquad \text{(A17)}$$

From equation (A17) it is seen that for the angle integrated case the matrix element separates into an atomic part given by the wavy brackets and a wave vector dependent "band-structure" part given by the sum. This latter part is exactly the total d-projection of the density of states.

APPENDIX B: TRANSPORT TERM

In evaluating the transport term we have assumed that the inelastic mean free path is much less than the photon absorption depth. The transport factor for excited electrons is then given by[1]

$$D_f(\vec{k}) \sim (\vec{s} \cdot \vec{\nabla}_k \, E_f(\vec{k})) \, \tau(E_f) \qquad \text{(B1)}$$

where $\vec{s}$ is a unit vector normal to the surface and $\tau(E_f)$ is the inelastic scattering lifetime in the "random-$\vec{k}$" or "phase-space" approximation.[25] Assuming the lifetime $\tau(E_f)$ to be a slowly varying function of the electron energy and taking the free electron value for the group velocity we can approximate $D_f(\vec{k})$ for a polycrystalline sample by

$$D_f(\vec{k}) \sim |\vec{q}| \tag{B2}$$

Since the photon energies used in our study are much larger than the width of the d-band the effect of the transport term (B2) on the calculated PED's (equation (1)) is very small.

APPENDIX C: CALCULATION OF THE PED's

The PED's were calculated on a mesh of 308 points in the 1/48 of the BZ defined by $k_y > k_x > k_z \geqslant 0$. Calculations carried out at a larger number of points ($\leqslant 1729$) indicated that a 308 point mesh was sufficient. In evaluating equation (1) the following steps were taken. At a given $\vec{k}$ point all initial ($E_j(\vec{k})$) and final ($E_f(\vec{k})$) energies were calculated. The energy conserving δ-function in equation (1) was treated by demanding that $E_f(\vec{k}) - E_j(\vec{k}) - \hbar\omega < W$. We chose $W = 0.01 \, E_f(\vec{k})$ but it was found that the calculated PED's were insensitive to the actual value of W. A similar observation was made by Janak et. al.[26] who found their calculations to be insensitive to broadening of the electron states. For each pair of initial and final state energies that satisfied the energy conserving δ-function in equation (1) a transition matrix element $|t_{fj}|^2$ was calculated. The product $|t_{fj}|^2 \, D_f(\vec{k})$ was taken as a weight factor for the density of states calculation. k-integration was performed using the Gilat-Raubenheimer method.[27] The PED's were then

convoluted with a 0.5 eV FWHM Gaussian to account for experimental
resolution and lifetime broadening of the hole states. The density
of (initial) states was calculated according to

$$D(E) \sim \int_{BZ} d^3k \sum_j \delta(E - E_j(\vec{k})).$$
(C1)

FOOTNOTES AND REFERENCES

1. For a recent review see D. E. Eastman in Proc. IV International Conference on Vacuum Ultraviolet Radiation Physics. Hamburg, July 1974, ed. E. Koch, R. Haensel, and C. Kunz (Pergamon, Vieweg 1974).

2. This is most easily seen for the case of free electron final states where the number of final states increases as the square root of photon energy.

3. For a recent review see C. R. Brundle, Surface Science 48, 99 (1975).

4. P. J. Feibelman and D. E. Eastman, Phys. Rev. B10, 4932 (1974).

5. F. C. Brown, R. Z. Bachrach, S. B. M. Hagström, N. Lien, and C. H. Pruett in Reference 1, p. 785.

6. P. W. Palmberg, J. Electron Spectrosc. 5, 691 (1974).

7. a) C. S. Fadley and D. A. Shirley, Electronic Density of States, Nat. Bur. Stds. Special Publication 323, 163 (1971).

   b) I. Lindau and L. Wilson, Phys. Lett. 42A, 279 (1972).

   c) G. K. Wertheim, D. N. E. Buchanan, N. V. Smith, and M. M. Traum, Phys. Lett. 49A, 191 (1974).

8. The various significant contributions which lead to this semiclassical model are listed in Reference 4.

9. We are aware of only one band structure calculation which extends to ~150 eV above the Fermi level, namely, V. Hoffstein and D. S. Boudreaux, Phys. Rev. B2, 3013 (1970), who calculated energy bands for Aℓ using a pseudopotential method.

10. See for example L. Pincherle, Electronic Energy Bands in Solids, (MacDonald, London, 1971), pp. 104 - 108.

11. N. V. Smith, Phys. Rev. B3, 1862 (1971).

12. L. Hodges, H. Ehrenreich, and N. D. Lang, Phys. Rev. 152, 505 (1966); H. Ehrenreich and L. Hodges in Methods in Computational Physics, edited by B. Alder, S. Fernbach, and M. Rotenberg (Academic, New York, 1968), Vol. 8, p. 149.

13. J. W. Gadzuk, Phys. Rev. B10, 5030 (1974).

14. E. Clementi and C. Roetti, Atomic Data and Nuclear Data Tables 14, 177 (1974).

15. We assume that our sample did not show any preferential crystalline orientation. For a true-polycrystalline sample the polarization of the incoming synchrotron light averages out with respect to the various crystalline orientations.

16. These emission directions lead to the "primary cones" in Mahan's terminology (G. D. Mahan, Phys. Rev. B2, 4334 (1970).

17. For wave functions with a radial node, so called Cooper-Minima (J. W. Cooper, Phys. Rev. Lett. 13, 762 (1964)) may arise and the transition strength may vary strongly with energy. Effects of this kind have been observed by us for the 4d valence band in Ag metal. These results will be published separately.

18. V. V. Nemoshkalenko, B. G. Aleshin, Yu. N. Kucherenko, and L. M. Sheludchenko, Solid State Comm. 15, 1745 (1974).

19. F. R. McFeely, J. Stöhr, G. Apai, P. S. Wehner, and D. A. Shirley, submitted for publication.

20. W. D. Grobman, D. E. Eastman, and J. L. Freeouf, Phys. Rev. B12, 4405 (1975).

21. B. Feuerbacher and R. F. Willis, J. Phys. C 9, 169 (1976).

22. Recently I. Lindau, P. Pianetta, K. Y. Yu, and W. E. Spicer, Phys. Rev. B13, 492 (1976), reported photoemission results on polycrystal-line Au. In this case cross section effects due to the radial nodes of the 5d wave function may be present. Similar cross section effects have also been observed by us for the case of Ag(4d).

23. A. Liebsch, Phys. Rev. B13, 544 (1976).

24. P. M. Morse and H. Feshbach, Methods of Theoretical Physics, McGraw-Hill, New York (1953), p. 1573.

25. E. Kane, Phys. Rev. 159, 624 (1967).

26. J. F. Janak, A. R. Williams, and V. L. Moruzzi, Phys. Rev. B11, 1522 (1975).

27. G. Gilat and L. J. Raubenheimer, Phys. Rev. 144, 390 (1966).

Table I.   Momentum Matrix Elements Between d and p Orbitals.*

$< d_1 \mid L_x \mid p_2 > = 1/\sqrt{5}$	$< d_1 \mid L_y \mid p_1 > = 1/\sqrt{5}$	$< d_2 \mid L_z \mid p_2 > = 1/\sqrt{5}$
$< d_3 \mid L_x \mid p_3 > = 1/\sqrt{5}$	$< d_2 \mid L_y \mid p_3 > = 1/\sqrt{5}$	$< d_3 \mid L_z \mid p_1 > = 1/\sqrt{5}$
$< d_4 \mid L_x \mid p_1 > = 1/\sqrt{5}$	$< d_4 \mid L_y \mid p_2 > = -1/\sqrt{5}$	$< d_5 \mid L_z \mid p_3 > = 2/\sqrt{15}$
$< d_5 \mid L_x \mid p_1 > = -1/\sqrt{15}$	$< d_5 \mid L_y \mid p_2 > = -1/\sqrt{15}$	

*   Here we have defined $d_1 = d_{xy}$, $d_2 = d_{yz}$, $d_3 = d_{xz}$, $d_4 = d_{x2-y2}$,

   $d_5 = d_{3z2-r2}$, and $p_1 = p_x$, $p_2 = p_y$, $p_3 = p_z$.

FIGURE CAPTIONS.

Figure 1.   Photoemission spectra of the 3d valence band of Cu for a series
            of photon energies. The data have been corrected for the de-
            cay in photon flux from the synchrotron but no background
            subtraction or deconvolution has been carried out.

Figure 2.   a) X-ray photoemission spectrum ($A\ell$ K_α radiation) of the
            Cu valence band recorded on an Hewlett-Packard spectrometer.
            b) The Cu 3d density of states (equation (C1)), using Smiths[11]
            parameters. The dashed curve represents the original density
            of states. The solid curve is a convolution with a FWHM =
            0.5 eV Gaussian.

Figure 3.   a) PED calculated for Cu 3d assuming k-conservation (direct
            transitions)
            b) Experimental results for Cu. The original data shown in
            Figure 1 have been corrected for their inelastic background.
            c) PED calculation for Cu assuming k-broadening in the final
            state. The broadening factor B is discussed in the text.

Figure 4.   Square of the radial dipole matrix element $\overline{|t_{fj}|^2}$ for Cu 3d
            as a function of the kinetic energy of the photoelectron.
            PW means plane wave, OPW means orthogonalized plane wave
            final state.

Figure 5.   Calculated PED for Cu 3d at $h\nu$ = 50 eV and 90 eV according
            to equation (1). The solid lines were calculated with the
            matrix elements given by equation (4). The dashed lines were
            calculated with an angle integrated (or essentially constant)
            matrix element given by equation (A17).

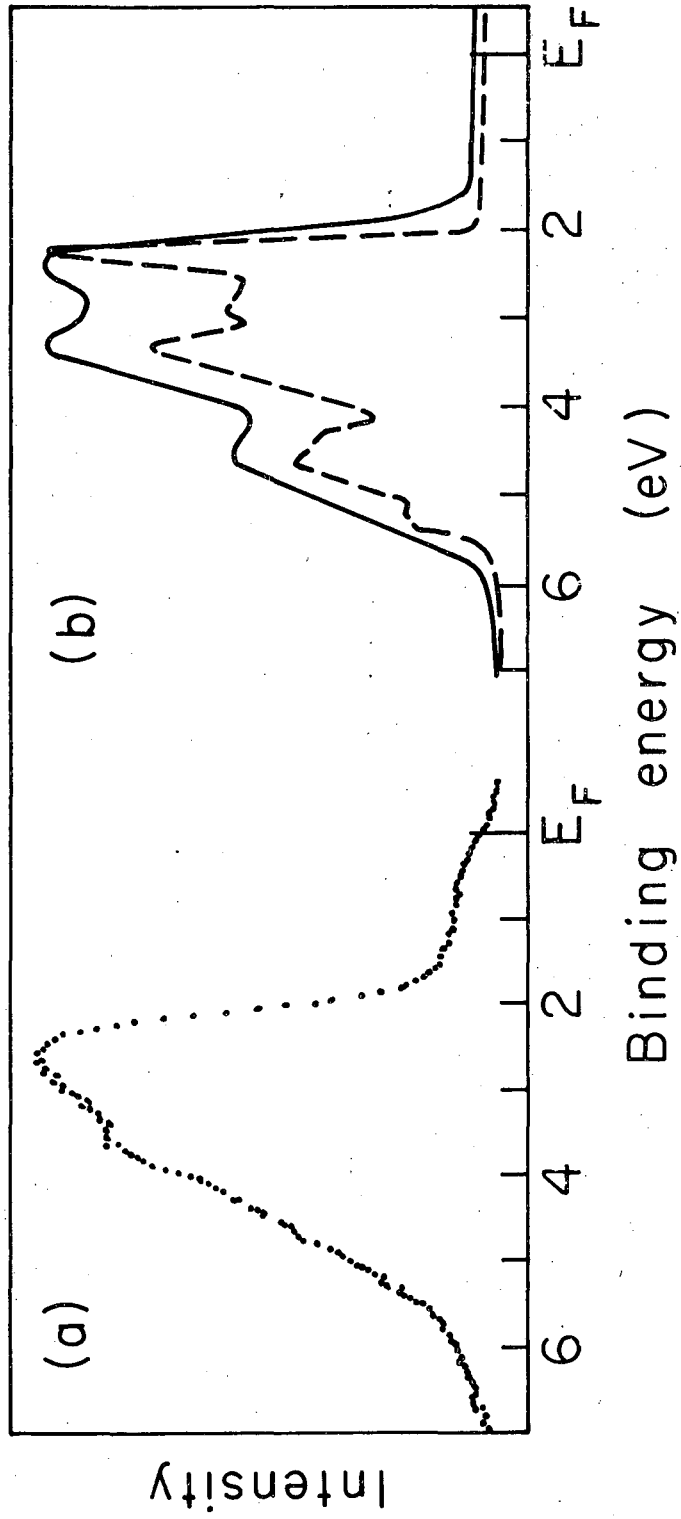a) PED's convoluted with a FWHM = 0.5 eV Gaussian.

b) Unconvoluted PED's.

Figure 6. Calculated PED for Cu 3d at hν = 50 eV as a function of momentum broadening in the final state (B).

a) PED's convoluted with a FWHM = 0.5 eV Gaussian.

b) Unconvoluted PED's.

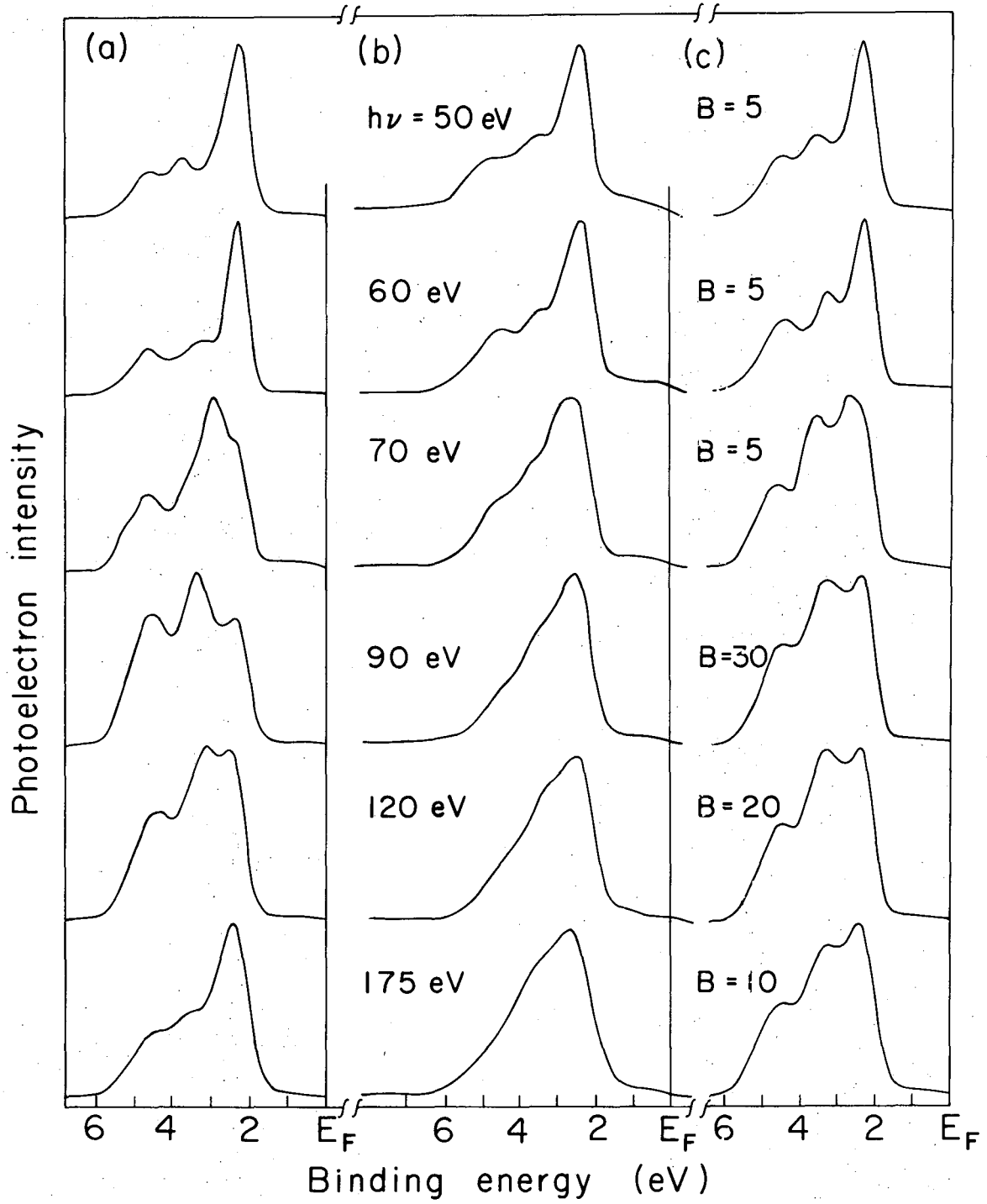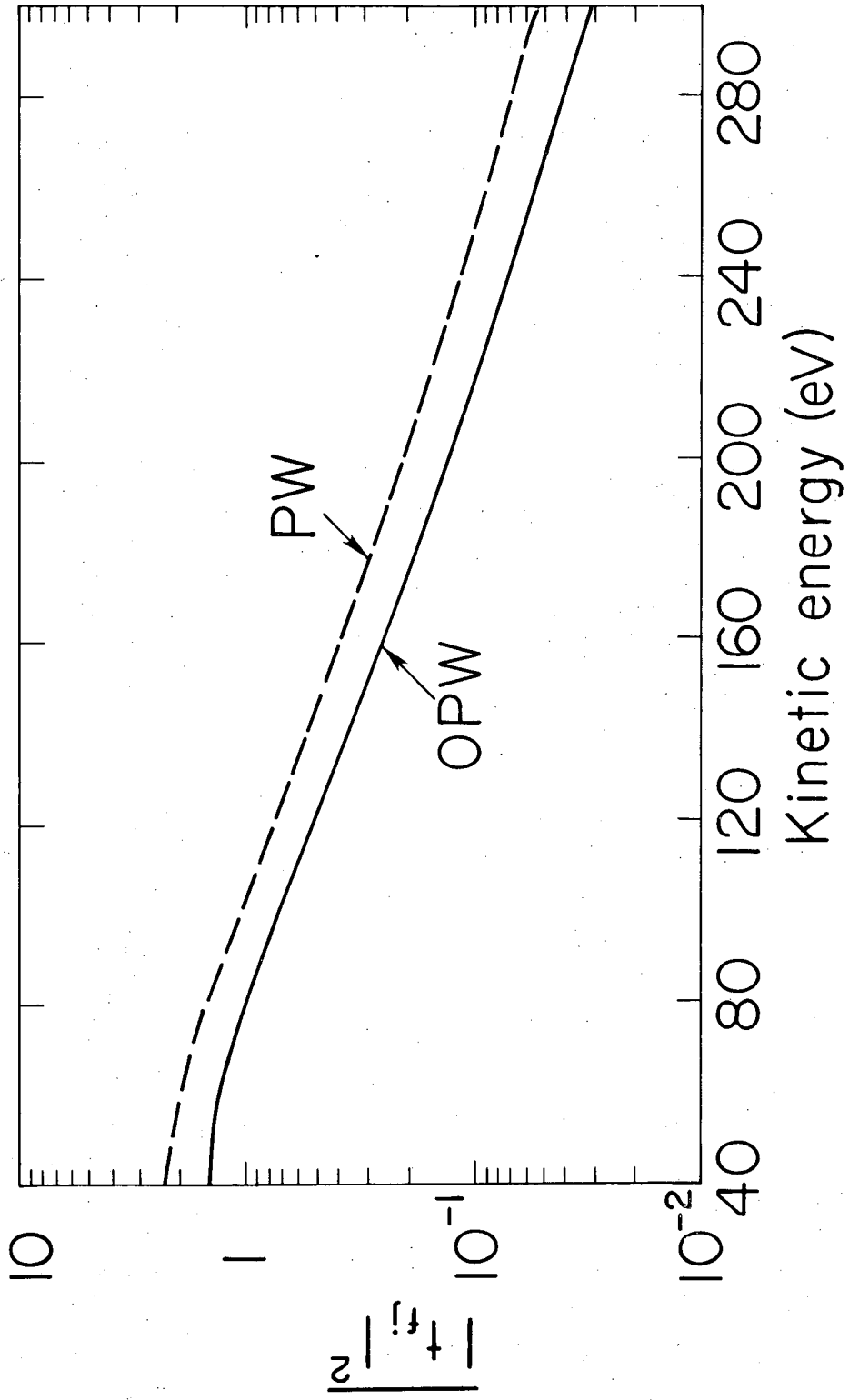Fig. 1

(b)

(a)

Intensity

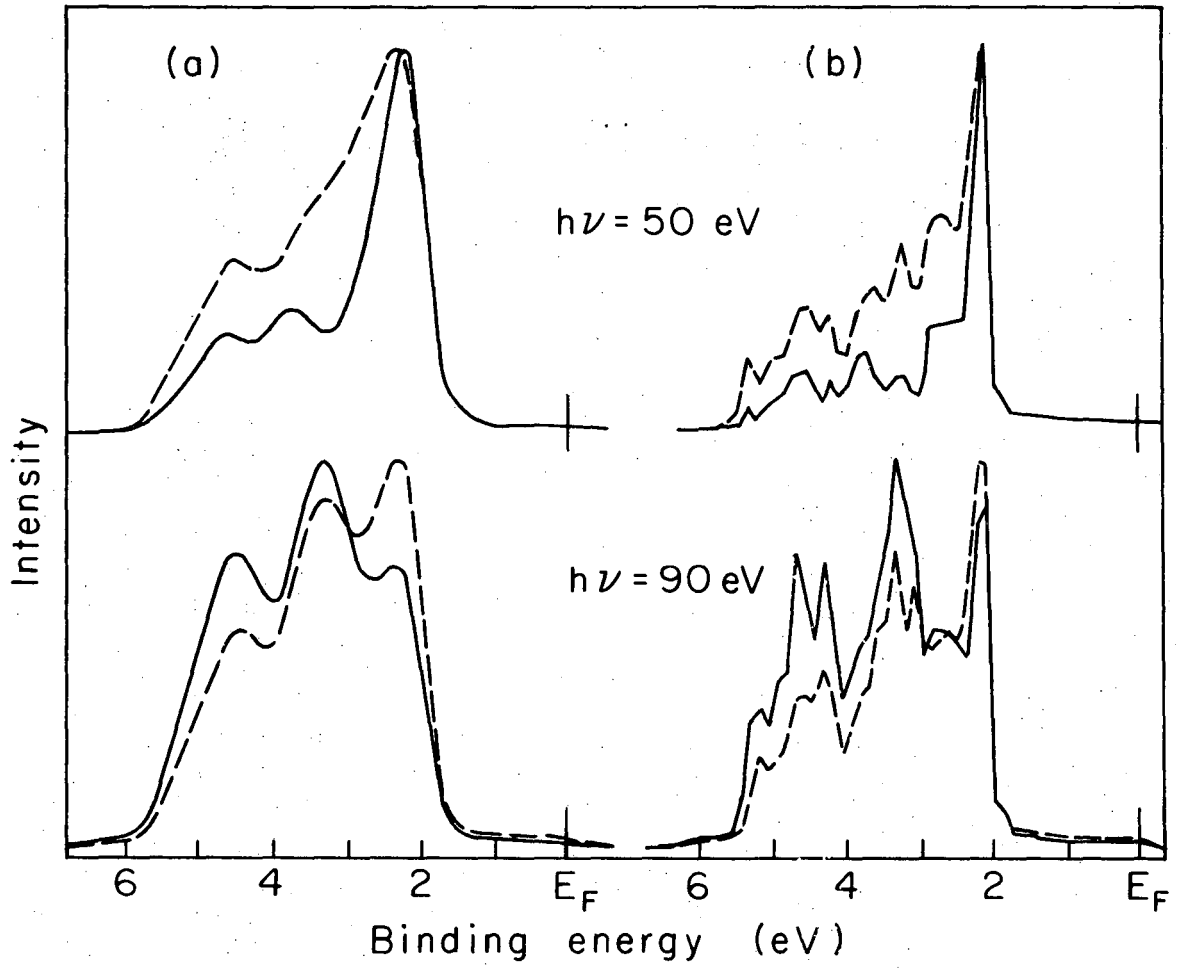Binding energy (eV)

E_F

E_F

XBL761-2107

Fig. 2

Fig. 3

XBL 761-2110

Fig. 4

XBL761-2113

XBL 761-2108

Fig. 5

$h\nu = 50\,eV$

B = 25
B = 10
B = 5
B = 0

(a)

(b)

Binding energy (eV)

Intensity

E_F

XBL761-2109

Fig. 6